Electronic Supplementary Material (ESI) for Materials Chemistry Frontiers.


Supporting Information for

# Covalent organic frameworks confining ultra-dense hydrated hydrogen-bond networks for efficient intrinsic proton conduction

Ruo-Meng Zhu‡, Jia-Xing Fu‡, Liang-Hui Chen, Jing-Dong Feng and Zhi-Guo Gu*

Key Laboratory of Synthetic and Biological Colloids, Ministry of Education, School of Chemical and Material Engineering, Jiangnan University, Wuxi 214122, P.R. China
E-mail: zhiguogu@jiangnan.edu.cn.

# Table of Contents

## 1. General synthetic procedures

### 1.1. Synthesis of 1,5-diformyl-2,6-dihydroxynaphthalene (2,6-DHNA)

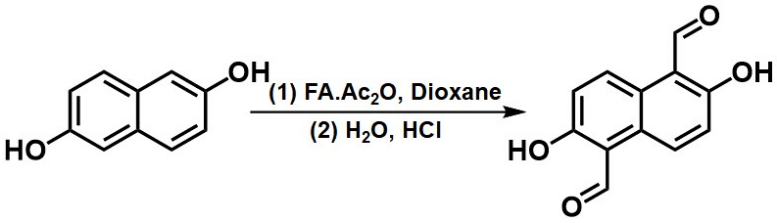


**Fig. S1** Synthesis of 2,6-DHNA.

2,6-DHNA was synthesized according to the reported method with slight modification.[1] Formamidine acetate (2.81 g, 27 mmol) and 80 ml of dioxane were added and stirred to gradually increase the temperature to 95 °C in a round bottom flask. Then, the acetic anhydride (5.1 mL, 54 mmol) was added and kept stirring until all the formamidine acetate completely dissolved. Next, 2,6-naphthalenediol (540 mg, 3.375 mmol) was added and the flask was sealed. The whole reaction lasted for two days. After cooling to room temperature, the remaining solvent was evaporated under reduced pressure at 60 °C. 80 mL of water was added and stirred for 4 h at 60 °C. The hydrochloric acid solution (1 M, 80 mL, 15 mmol) was then added and kept stirring for 18 h. The final precipitate was collected by filtration and washed with hexanes. The crude powder was purified by column chromatography using dichloromethane:hexanes (50%:50%) as the eluent. A pure product as a yellow powder was obtained (574.5 mg, 2.50 mmol). Yield: 74%.

$^{1}$H NMR (400 MHz, $CDCl_3$) $\delta$ 11.59, 10.76, 9.14, 7.36. $^{13}$C NMR (101 MHz, DMSO) $\delta$ 193.21, 162.02, 132.84, 126.33, 121.80,113.80.

### 1.2. Synthesis of 1,4-diformyl-2,3-dihydroxynaphthalene (2,3-DHNA)

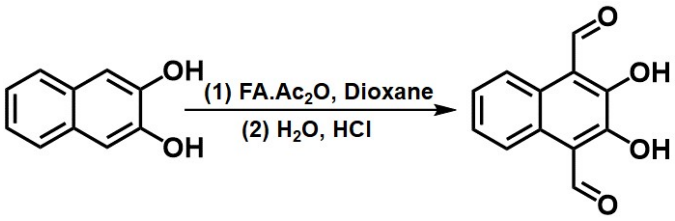


**Fig. S2** Synthesis of 2,3-DHNA.

2,3-DHNA was synthesized according to the reported procedure with slight modification.[1] Formamidine acetate (2.81 g, 27 mmol) and 150 ml of dioxane were added and stirred to gradually increase the temperature to 95 °C in a round bottom flask. Then, the acetic anhydride (5.1 mL, 54 mmol) was added and kept stirring until all the formamidine acetate completely dissolved. Next, 2,3-naphthalenediol (540 mg, 3.375 mmol) was added and the flask was sealed. The whole reaction lasted for two days. After cooling to room temperature, the remaining solvent was evaporated under reduced pressure at 60 °C. 80 mL of water was added and stirred for 4 h at 60 °C. The hydrochloric acid solution (1 M, 80 mL, 80 mmol) was then added and kept stirring for 18 h. The final precipitate was collected by filtration and washed with hexanes. The crude powder was purified by column chromatography using dichloromethane (100%) as the eluent. A pure product as a yellow powder was obtained (345.6 mg, 1.586 mmol). Yield: 47%.

$^{1}$H NMR (400 MHz, $CDCl_3$) $\delta$ 12.96, 10.89, 8.37, 7.60. $^{13}$C NMR (101 MHz, DMSO): $\delta$ 194.59, 154.70, 126.74, 125.84, 122.74, 117.49.

### 1.3. Synthesis of 1,3,5-tris(4-aminophenyl) triazine (TAPT)

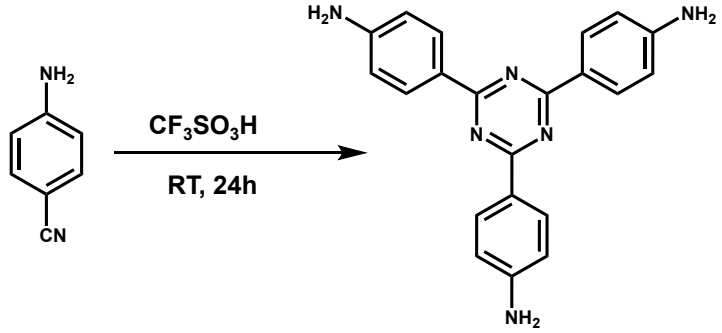


**Fig. S3** Synthesis of TAPT.

TAPT was synthesized according to the reported method with slight modification.[2] 4-aminobenzonitrile (0.76 g, 6.5 mmol) was taken in a 10 mL round bottom fask and then then flash frozen in a liquid nitrogen bath. Trifluoromethanesulfonic acid (2 mL, 22.2 mmol) was added dropwise in an ice bath. The mixture was stirred for 24 h at room temperature in inert atmosphere. After that, add water to precipitate and neutralize by 1M NaOH solution to reach pH = 7. The resulting precipitate was collected by filtration, washed with water to obtain pale yellow powder (0.605 g, 1.07 mmol). Yield: 79%.

$^{1}$H NMR (400 MHz, DMSO) $\delta$ 8.35, 0, 6.70, 5.87. $^{13}$C NMR (101 MHz, DMSO) $\delta$ 170.12, 153.50, 130.71, 123.62, 113.74.

## 2. Synthesis conditions of COFs

### 2.1. Synthesis conditions of 2,6-DHNA-TA

**Tab. S1** Synthetic conditions screened for synthesizing 2,6-DHNA-TA.

| Entry | Solvents | *T* (°C) | Catalyst | Crystallinity |
|---|---|---|---|---|
| (1) | Mesitylene /Dioxane = 0.2/1.8 | 120 | 6 M Acetic acid | No |
| (2) | Mesitylene /Dioxane = 0.4/1.6 | 120 | 6 M Acetic acid | No |
| (3) | Mesitylene /Dioxane = 0.8/1.2 | 120 | 6 M Acetic acid | No |
| (4) | Mesitylene /Dioxane = 1.0/1.0 | 120 | 3 M Acetic acid | Low |
| (5) | Mesitylene /Dioxane = 1.2/0.8 | 120 | 6 M Acetic acid | No |
| (6) | Mesitylene /Dioxane = 1.6/0.4 | 120 | 9 M Acetic acid | High |
| (7) | o-dichlorobenzene/n-butanol = 0.2/1.8 | 120 | 6 M Acetic acid | No |
| (8) | o-dichlorobenzene/n-butanol = 0.4/1.6 | 120 | 6 M Acetic acid | No |
| (9) | o-dichlorobenzene/n-butanol = 0.8/1.2 | 120 | 6 M Acetic acid | Low |
| (10) | o-dichlorobenzene/n-butanol = 1/1 | 120 | 6 M Acetic acid | Moderate |
| (11) | o-dichlorobenzene/n-butanol = 1.2/0.8 | 120 | 6 M Acetic acid | No |
| (12) | o-dichlorobenzene/n-butanol = 1.6/0.4 | 120 | 6 M Acetic acid | No |

## 2.2. Synthesis conditions of 2,3-DHNA-TA

**Tab. S2** Synthetic conditions screened for synthesizing 2,3-DHNA-TA.

| Entry | Solvents | T (°C) | Catalyst | Crystallinity |
|---|---|---|---|---|
| (1) | Mesitylene /Dioxane = 0.2/1.8 | 120 | 6 M Acetic acid | No |
| (2) | Mesitylene /Dioxane = 0.4/1.6 | 120 | 6 M Acetic acid | No |
| (3) | Mesitylene /Dioxane = 0.8/1.2 | 120 | 6 M Acetic acid | No |
| (4) | Mesitylene /Dioxane = 1.0/1.0 | 120 | 3 M Acetic acid | No |
| (5) | Mesitylene /Dioxane = 1.6/0.4 | 120 | 9 M Acetic acid | No |
| (6) | Mesitylene /Dioxane = 1.7/0.3 | 120 | 9 M Acetic acid | High |
| (7) | Mesitylene /Dioxane = 1.9/0.1 | 120 | 9 M Acetic acid | Low |
| (8) | o-dichlorobenzene/n-butanol = 0.8/1.2 | 120 | 6 M Acetic acid | No |
| (9) | o-dichlorobenzene/n-butanol = 0.4/1.6 | 120 | 6 M Acetic acid | No |
| (10) | o-dichlorobenzene/n-butanol = 1/1 | 120 | 6 M Acetic acid | No |
| (11) | o-dichlorobenzene/n-butanol = 1.6/0.4 | 120 | 6 M Acetic acid | No |
| (12) | o-dichlorobenzene/n-butanol = 1.2/0.8 | 120 | 6 M Acetic acid | No |

## 2.3. FT-IR spectra

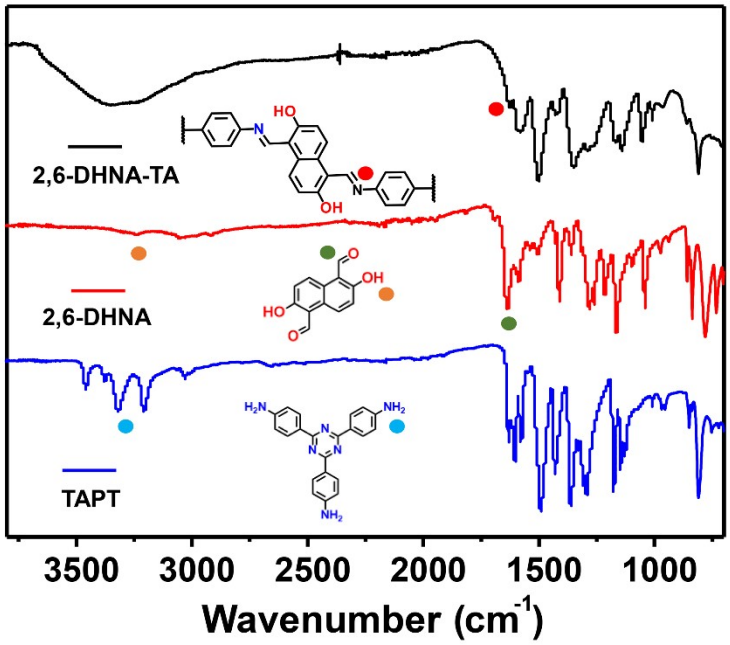


**Fig. S4** FT-IR spectra of TAPT, 2,6-DHNA and 2,6-DHNA-TA.

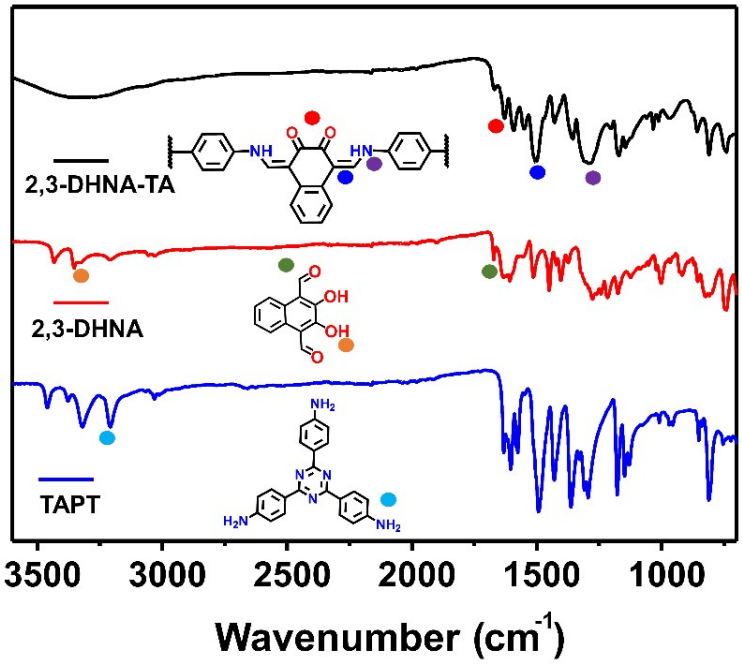


**Fig. S5** FT-IR spectra of TAPT, 2,3-DHNA and 2,3-DHNA-TA.

## 2.4. SEM and TEM images of COFs

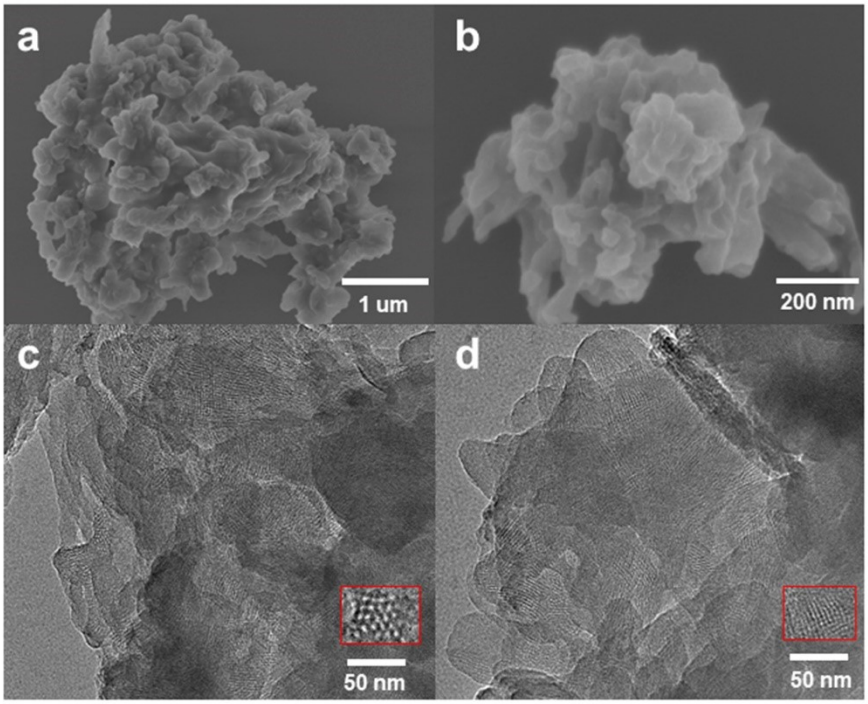


**Fig. S6** (a,b) SEM and (c,d) TEM images of 2, 6-DHNA-TA.

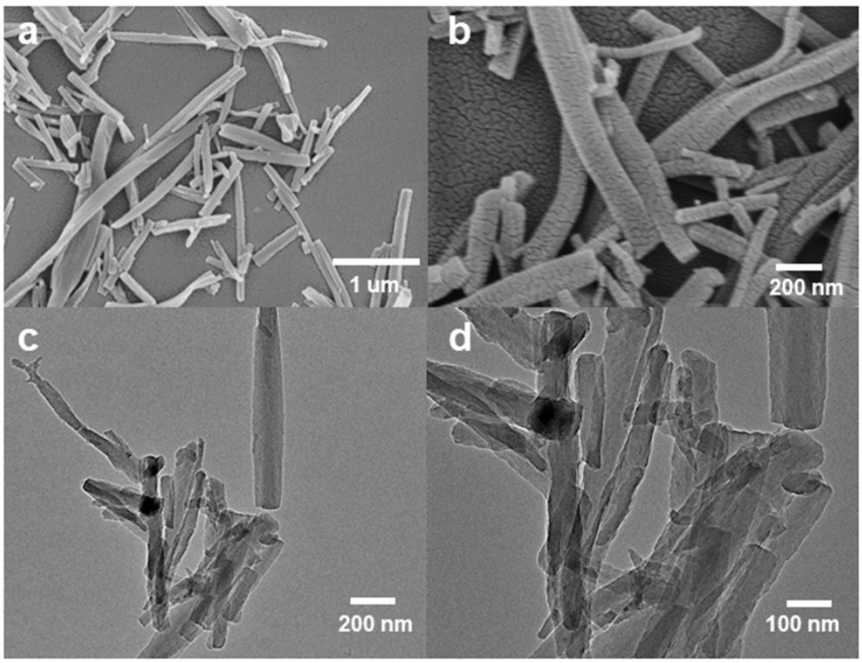


**Fig. S7** (a,b) SEM and (c,d) TEM images of 2, 3-DHNA-TA.

## 2.5. Pore size distribution

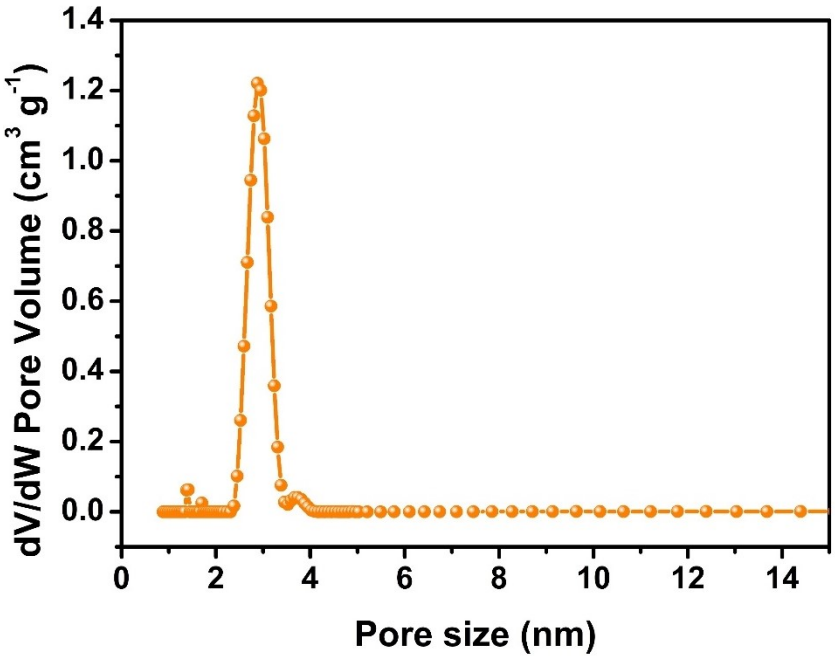


**Fig. S8** Pore size distribution of 2,6-DHNA-TA.

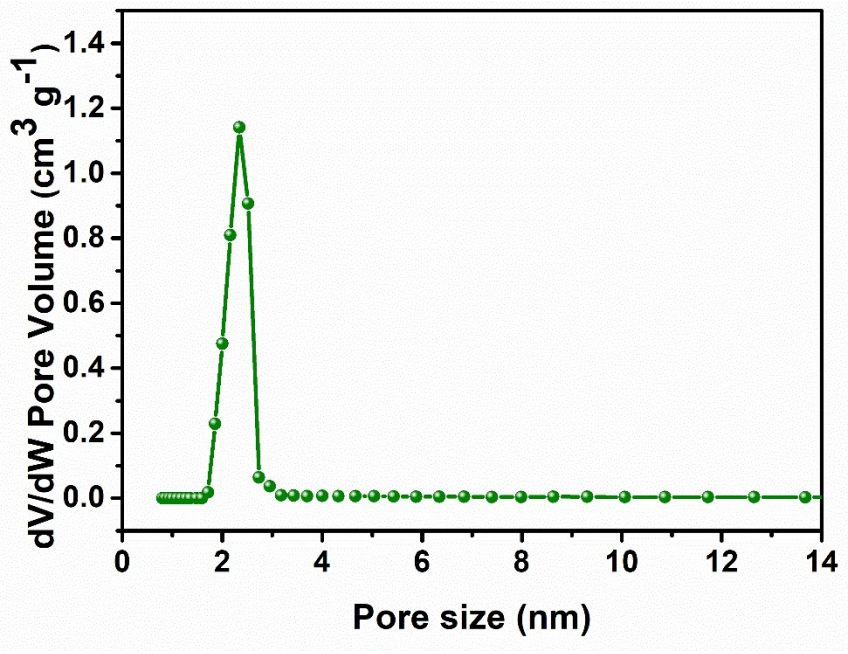


**Fig. S9** Pore size distribution of 2,3-DHNA-TA.

### 2.6. Structure simulation of COFs

Structural model of COFs given in the text was generated by using the Materials Visualizer module within Materials Studio (Material Studio ver. 7.0, Accelrys Software Inc.). Unit cell dimension was set to the theoretical parameters. TAPT linkers were first located at the positions indicated by the specific topologies. TAPT linkers were then linked by the 2,3-DHNA or 2,6-DHNA building units. The lattice models (e.g., cell parameters, atomic positions, total energies, total crystal stacking energy per layer and cohesive bulk energy per layer) were then fully optimized using Materials Studio Forcite molecular dynamics module (Universal Force Fields (UFF) using charges Qeq neutral1.0, Ewald summations) method.

#### 2.6.1. Simulated AA modes of 2,6-DHNA-TA

In the simulations, two possible structural forms (eclipsed stacking (AA) and staggered stacking (AB)) were constructed, and the respective corresponding theoretical PXRD profiles were compared with their experimental data.

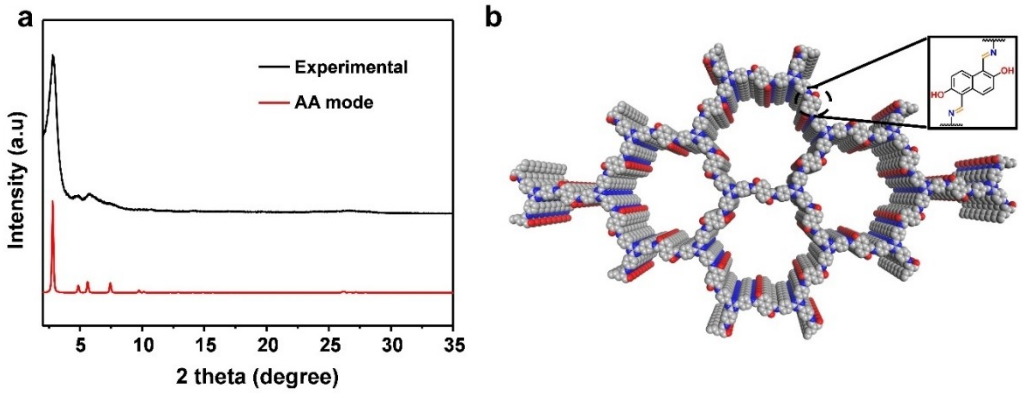


**Fig. S10** (a) Theoretical and experimental PXRD patterns for the AA stacking mode of 2,6-DHNA-TA; (b) eclipsed stacking AA mode of 2,6-DHNA-TA.

#### 2.6.2. Simulated AB modes of 2,6-DHNA-TA

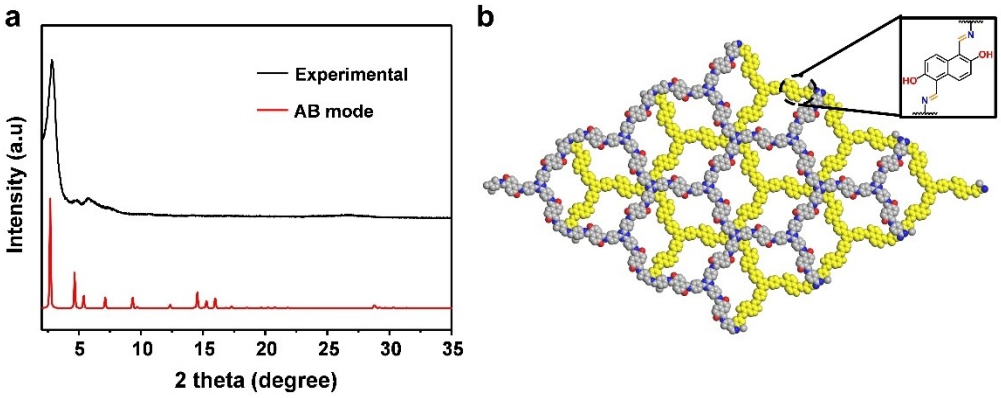


**Fig. S11** (a) Theoretical and experimental PXRD patterns for the AB stacking mode of 2,6-DHNA-TA; (b) Staggered stacking AB mode of 2,6-DHNA-TA.

### 2.6.3. Simulated AA modes of 2,3-DHNA-TA

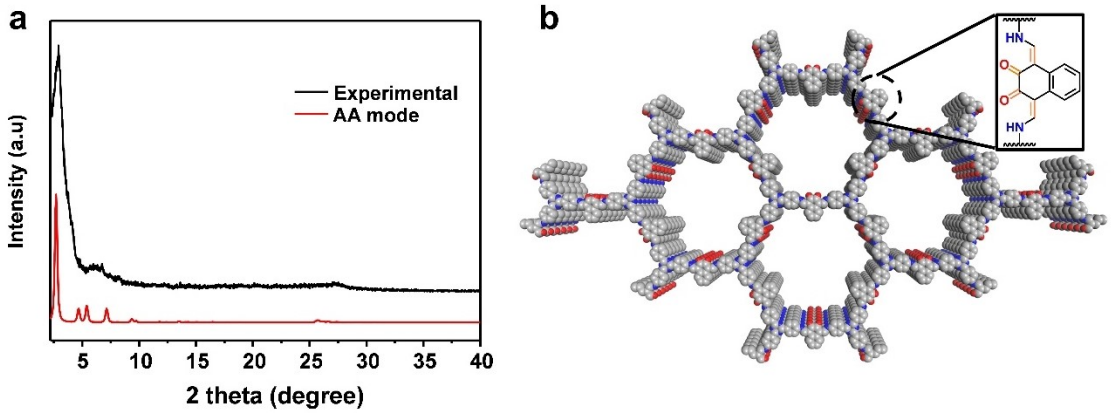


**Fig. S12** (a) Comparison of theoretical PXRD patterns and experimental results for the AA stacking mode of 2,3-DHNA-TA; (b) eclipsed stacking AA mode of 2,3-DHNA-TA.

### 2.6.4. Simulated AB modes of 2,3-DHNA-TA

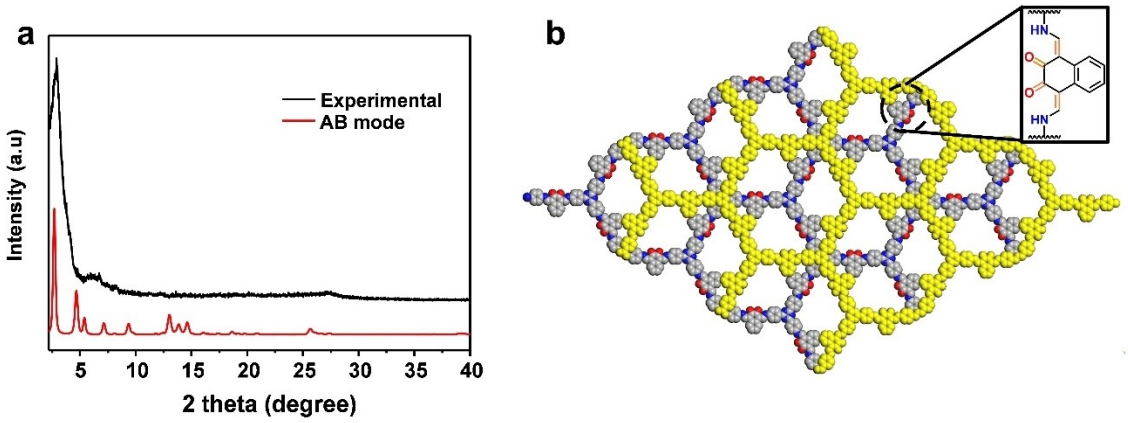


**Fig. S13** (a) Comparison of theoretical PXRD patterns and experimental results for the AB stacking mode of 2,3-DHNA-TA; (b) Staggered stacking AB mode of 2,3-DHNA-TA.

**Tab. S3** Atomistic coordinates of 2,6-DHNA-TA with AA stacking mode via Pawley refinement (space group *P6/M*, $a = b = 37.92$ Å, $c = 3.50$ Å, $\alpha = \gamma = 90°$ and $\beta = 120°$).

| Atom | x | y | z |
|---|---|---|---|
| C1 | 3.43094 | 1.43627 | 0 |
| C2 | 3.45906 | 1.42281 | 0 |
| C3 | 3.50128 | 1.45118 | 0 |
| C4 | 3.51443 | 1.49329 | 0 |
| C5 | 3.44397 | 1.47769 | 0 |
| C6 | 3.46789 | 1.56193 | 0 |
| O7 | 3.44466 | 1.38175 | 0 |
| C8 | 4.63911 | 1.34641 | 0 |
| N9 | 4.62626 | 1.30593 | 0 |
| C10 | 4.75123 | 1.39069 | 0 |
| C11 | 4.77979 | 1.3775 | 0 |
| C12 | 4.82145 | 1.40575 | 0 |
| C13 | 4.8351 | 1.44768 | 0 |
| C14 | 4.80663 | 1.46084 | 0 |
| C15 | 4.76497 | 1.43256 | 0 |
| N16 | 4.87756 | 1.47741 | 0 |

**Tab. S4** Atomistic coordinates of 2,3-DHNA-TA with AA stacking mode via Pawley refinement (space group *P-62M*, $a = b = 37.79$ Å, $c = 3.48$ Å, $\alpha = \gamma = 90°$ and $\beta = 120°$).

| Atom | x | y | z |
|---|---|---|---|
| C1 | 0.29178 | 1.64584 | 1.5 |
| N2 | 0.31276 | 1.62542 | 1.5 |
| C3 | 0.3769 | 1.62331 | 1.5 |
| C4 | 0.41961 | 1.77556 | 1.5 |
| C5 | 0.441 | 1.8183 | 1.5 |
| C6 | 0.41989 | 1.84028 | 1.5 |
| C7 | 0.37697 | 1.81812 | 1.5 |
| C8 | 0.35561 | 1.77542 | 1.5 |
| N9 | 0.4442 | 1.55979 | 1.5 |
| C10 | 0.42756 | 1.51597 | 1.5 |
| C11 | 0.44911 | 1.49549 | 1.5 |
| C12 | 0.49467 | 1.51718 | 1.5 |
| C13 | 0.44896 | 1.42694 | 1.5 |
| C14 | 0.38335 | 1.42559 | 1.5 |
| C15 | 0.36225 | 1.38325 | 1.5 |
| O16 | 0.51476 | 1.55435 | 1.5 |

## 2.7. Chemical stability test

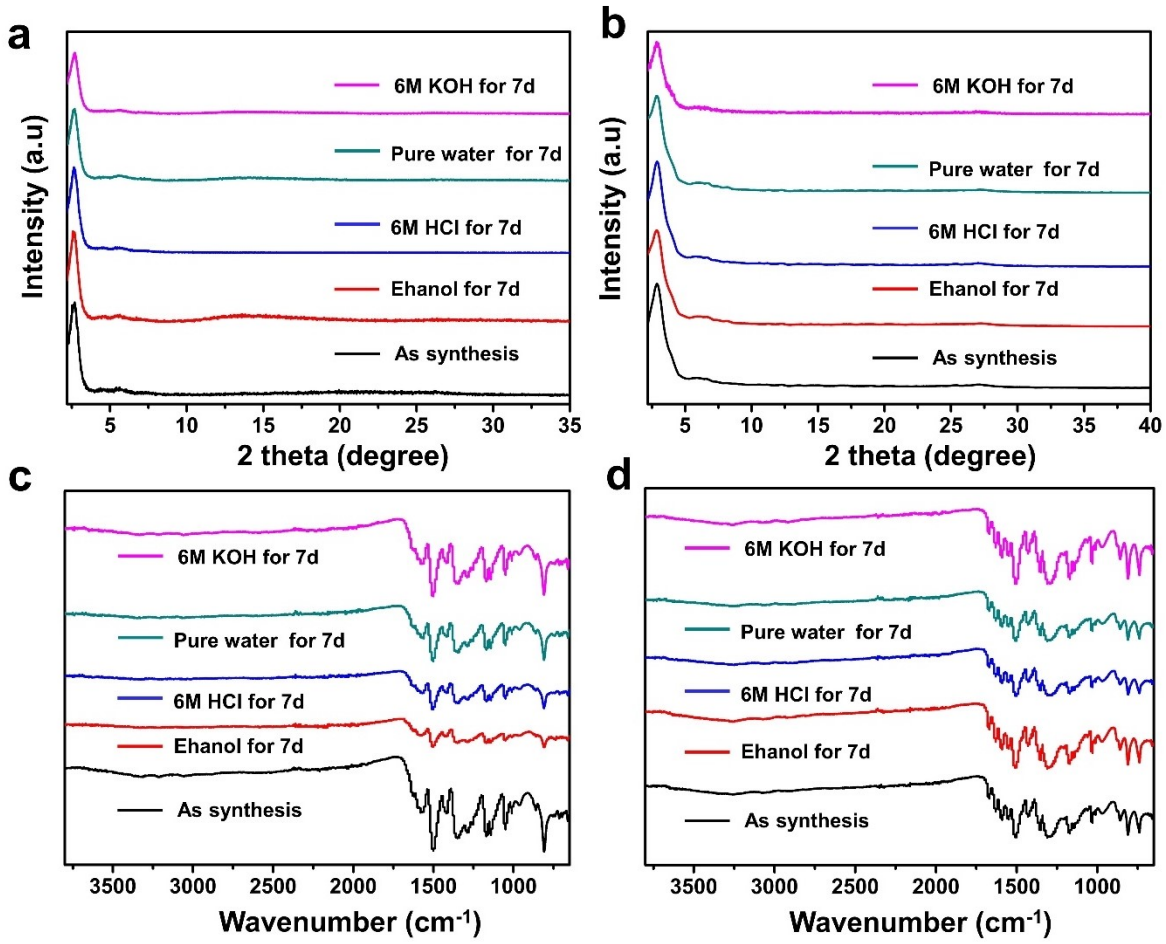


**Fig. S14** PXRD pattern of (a) 2, 6-DHNA-TA and (b) 2, 3-DHNA-TA before and after immersion in different solvents; FT-IR spectra of (c) 2, 6-DHNA-TA and (d) 2, 3-DHNA-TA before and after immersion in different solvents.

## 2.8. Thermogravimetric analysis

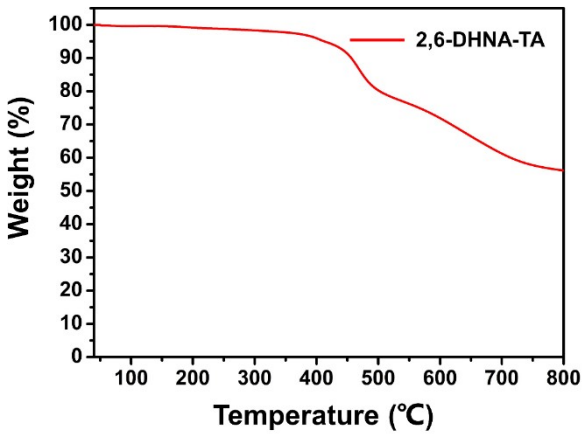


**Fig. S15** TGA profile of 2,6-DHNA-TA.

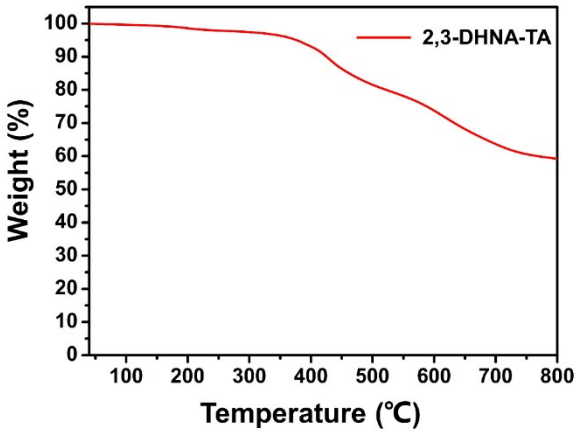


**Fig. S16** TGA profile of 2,3-DHNA-TA.

**Tab. S5** Comparison of the water capturing properties of typical COFs and MOFs that have been reported with the materials in this work.

| COF | Pore diameter (nm) | Water uptake (g $g^{-1}$) at $P/P_{sat}$ = 0.90-0.95 and 298 K | BET surface ($m^2$ $g^{-1}$) | Reference |
|---|---|---|---|---|
| TpPa-1 | 1.8 | 0.44 | 984 | [3] |
| TP-Azo | 2.7 | 0.41 | 942 | [3] |
| AB-COF | 1.3 | 0.40 | 1120 | [4] |
| TpBpy | 2.4 | 0.85 | 942 | [5] |
| 3D-CageCOF-1 | 0.86 and 0.5 | 0.32 | 1336 | [6] |
| TTA-TFB-COF | 1.5 | 0.52 | 1244 | [7] |
| TFPPy-PDA-COF | 2.1 | 0.62 | 1532 | [7] |
| S-COF | 2.3 | 0.42 | 1690 | [8] |
| FS-COF | 2.8 | 0.67 | 1652 | [8] |
| BT-COF | 2.4 | 0.52 | 1471 | [9] |
| DUT-175 | 1.9 | 0.72 | 1071 | [10] |
| DUT-176 | 2.2 | 0.48 | 1062 | [10] |
| Pythz-COF | 2.34 | 0.83 | 1571 | [11] |
| DHTA-Pa COF | 1.4 | 0.77 | 2099 | [12] |
| MOF-841 | 0.92 | 0.51 | 1390 | [13] |
| PIZOF-2 | 1.76 | 0.68 | 2080 | [13] |
| (Mg) MOF-74 | 1.1 | 0.6 | 1250 | [13] |
| COF-ok | 1.3 | 0.62 | 1194 | [14] |
| COF-pe | 1.5 | 0.5 | 795 | [14] |
| 2,3-DHNA-TA | 2.4 | 0.66 | 1424 | This work |
| 2,6-DHNA-TA | 2.8 | 0.86 | 1742 | This work |

## 3. Simulation details and validation of the GCMC

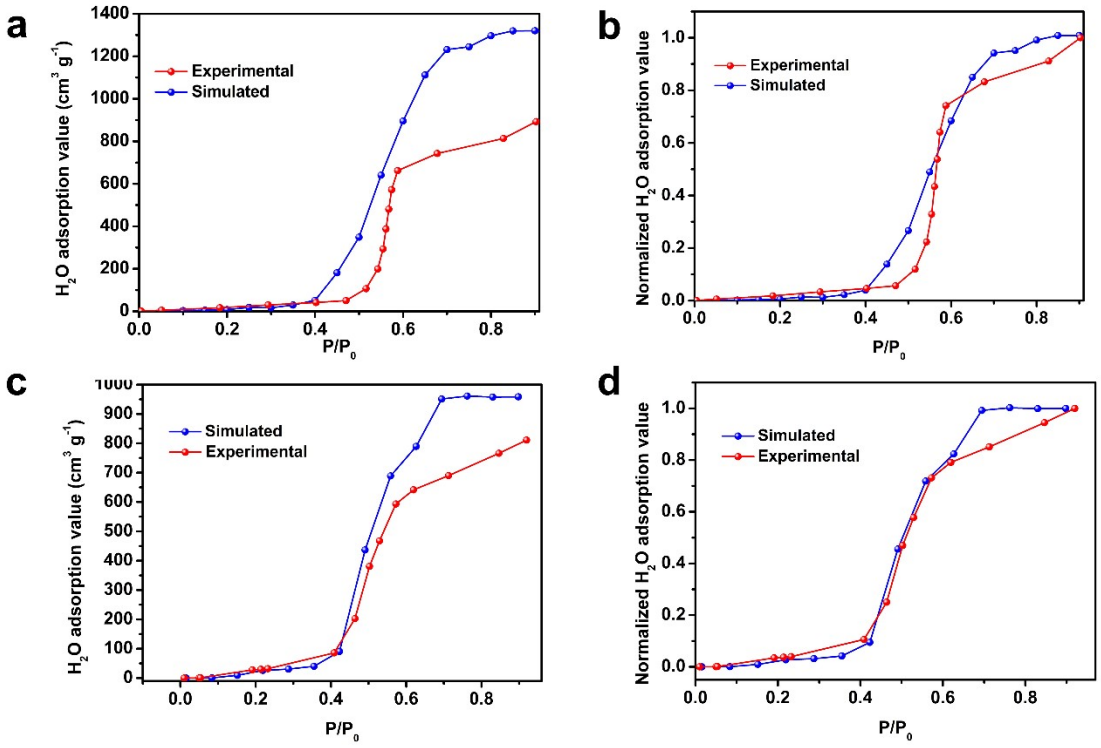


**Fig. S17** Simulated and measured water adsorption isotherms of (a) 2,6-DHNA-TA and (c) 2,3-DHNA-TA at 298 K; Normalized water adsorption isotherms of (b) 2,6-DHNA-TA and (d) 2,3-DHNA-TA at 298 K.

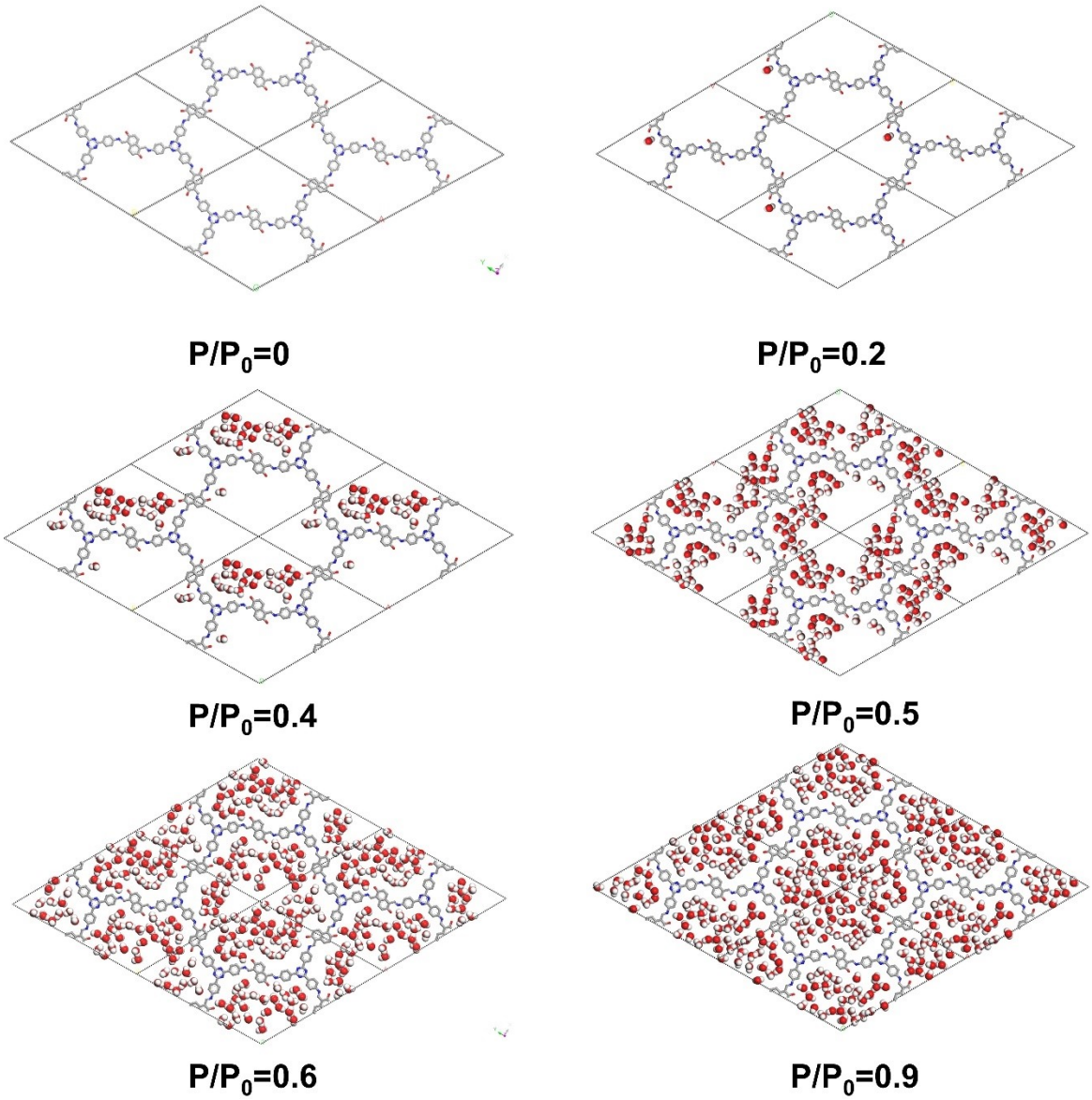


**Fig. S18** Distribution of the adsorbed water molecules in 2,6-DHNA-TA averaged over the GCMC configurations obtained at 298 K. C, gray; N, blue; O, red; H, white.

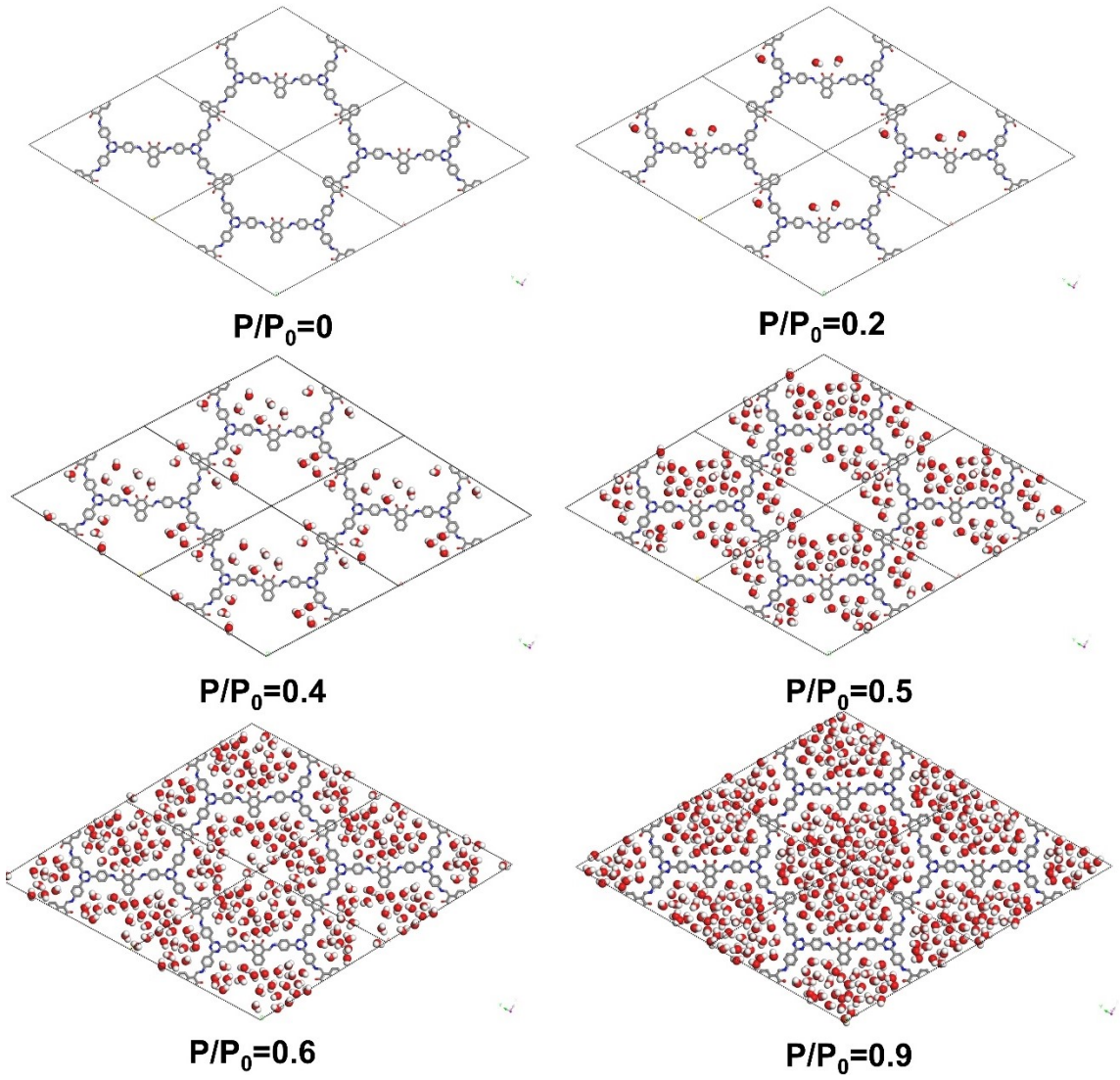


**Fig. S19** Distribution of the adsorbed water molecules in 2,3-DHNA-TA averaged over the GCMC configurations obtained at 298 K. C, gray; N, blue; O, red; H, white.

## 4. Proton conduction experiment

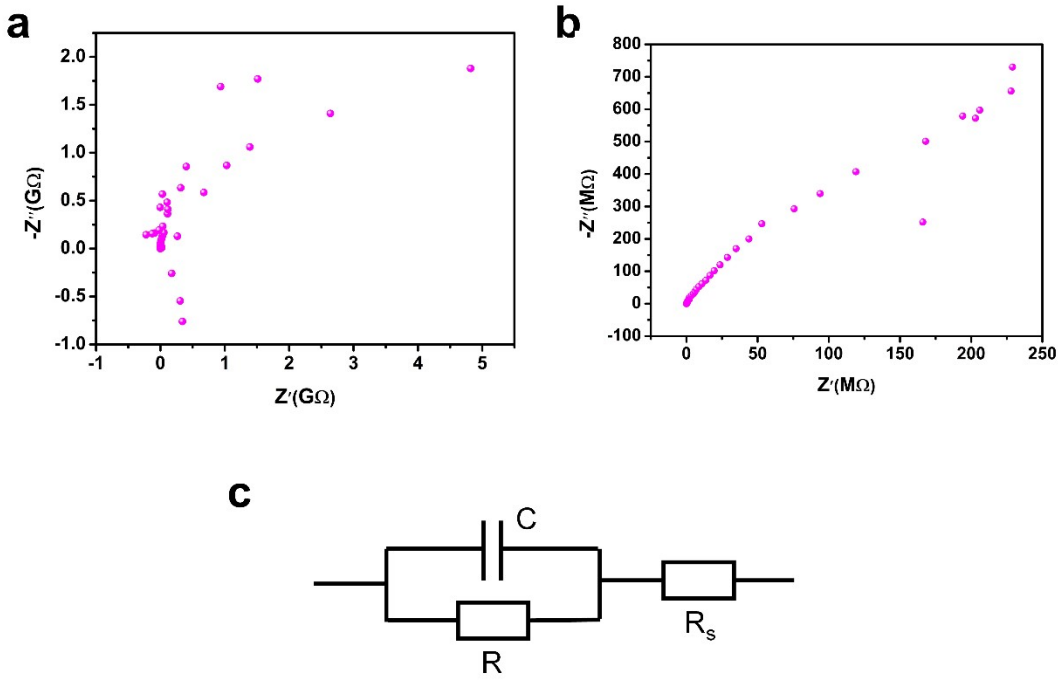


**Fig. S20** The impedance spectra of (a) 2, 6-DHNA-TA and (b) 2, 3-DHNA-TA at a low RH of 43%. (c) An equivalent circuit.

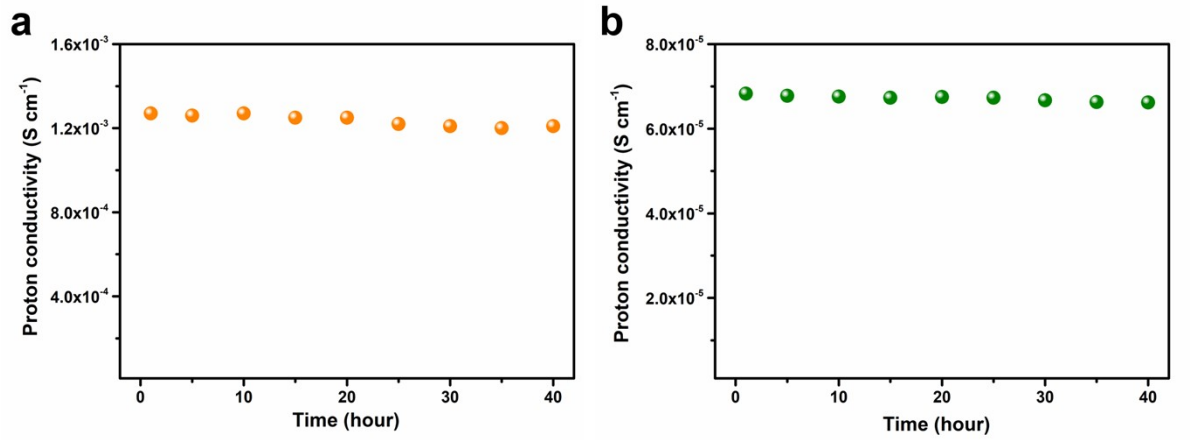


**Fig. S21** Long-term proton conductivity durability of (a) 2, 6-DHNA-TA and (b) 2, 3-DHNA-TA measurements at 353 K under 90% RH.

## 5. References


1. S. H. Mehr, H. Depmeier, K. Fukuyama, M. Maghami, M. J. MacLachlan, Formylation of phenols using formamidine acetate, *Org. Biomol. Chem.,* 2017, **15**, 581-583.
2. Z. Li, L. Sheng, H. Wang, X. Wang, M. Li, Y. Xu, H. Cui, H. Zhang, H. Liang, H. Xu, X. He, Three-dimensional covalent organic framework with ceq topology, *J. Am. Chem. Soc.,* 2020, **143**, 92-96.
3. B. P. Biswal, S. Kandambeth, S. Chandra, D. B. Shinde, S. Bera, S. Karak, B. Garai, U. K. Kharul, R. Banerjee, Pore surface engineering in porous, chemically stable covalent organic frameworks for water adsorption, *J. Mater. Chem. A*, 2015, **3**, 23664-23669.
4. L. Stegbauer, M. W. Hahn, A. Jentys, G. Savasci, C. Ochsenfeld, J. A. Lercher, B. V. Lotsch, Tunable water and $CO_2$ sorption properties in isostructural azine-based covalent organic frameworks through polarity engineering, *Chem. Mater.*, 2015, **27**, 7874-7881.
5. S. Karak, S. Kandambeth, B. P. Biswal, H. S. Sasmal, S. Kumar, P. Pachfule, R. Banerjee, Constructing ultraporous covalent organic frameworks in seconds via an organic terracotta process, *J. Am. Chem. Soc.,* 2017, **139**, 1856-1862.
6. Q. Zhu, X. Wang, R. Clowes, P. Cui, L. Chen, M. A. Little, A. I. Cooper, 3D cage COFs: A dynamic three-dimensional covalent organic framework with high-connectivity organic cage nodes, *J. Am. Chem. Soc.,* 2020, **142**, 16842-16848.
7. K. T. Tan, S. Tao, N. Huang, D. Jiang, Water cluster in hydrophobic crystalline porous covalent organic frameworks, *Nat. Commun.,* 2021, **12**, 6747.
8. X. Wang, L. Chen, S. Y. Chong, M. A. Little, Y. Wu, W. H. Zhu, R. Clowes, Y. Yan, M. A. Zwijnenburg, R. S. Sprick, A. I. Cooper, Sulfone-containing covalent organic frameworks for photocatalytic hydrogen evolution from water, *Nat. Chem.,* 2018, **10**, 1180-1189.
9. T. Zhou, L. Wang, X. Huang, J. Unruangsri, H. Zhang, R. Wang, Q. Song, Q. Yang, W. Li, C. Wang, K. Takahashi, H. Xu, J. Guo, PEG-stabilized coaxial stacking of two-dimensional covalent organic frameworks for enhanced photocatalytic hydrogen evolution, *Nat. Commun.,* 2021, **12**, 3934.
10. L. Gilmanova, V. Bon, L. Shupletsov, D. Pohl, M. Rauche, E. Brunner, S. Kaskel, Chemically stable carbazole-based imine covalent organic frameworks with acidochromic response for humidity control applications, *J. Am. Chem. Soc.,* 2021, **143**, 18368-18373.
11. S. Jiang, L. Meng, W. Ma, G. Pan, W. Zhang, Y. Zou, L. Liu, B. Xu, W. Tian, Dual-functional two-dimensional covalent organic frameworks for water sensing and harvestin, *Mater. Chem. Front.,* 2021, **5**, 4193-4201.
12. C. Sun, Y. Zhu, P. Shao, L. Chen, X. Huang, S. Zhao, D. Ma, X. Jing, B. Wang, X. Feng, 2D Covalent Organic Framework for Water Harvesting with Fast Kinetics and Low Regeneration Temperature, *Angew. Chem. Int. Ed.*, 2023, **62**, e202217103.
13. H. Furukawa, F. Gandara, Y. B. Zhang, J. Jiang, W. L. Queen, M. R. Hudson, O. M. Yaghi, Water adsorption in porous metal-organic frameworks and related materials, *J. Am. Chem. Soc.,* 2014, **136**, 4369-4381.
14. L. Chen L, W. K. Han, X. Yan, Z. G. Gu, A Highly Stable Ortho-Ketoenamine Covalent Organic Framework with Balanced Hydrophilic and Hydrophobic Sites for Atmospheric Water Harvesting, *Chem. Sus. Chem.,* 2022, **24**, e202201824.